Anisotropic mechanosensing by mesenchymal stem cells

Kyle Kurpinski*†, Julia Chu*, Craig Hashi*†, and Song Li*†‡

*Department of Bioengineering and Center for Tissue Engineering, and †UC Berkeley and UC San Francisco Joint Graduate Program in Bioengineering, University of California, Berkeley, CA 94720

Edited by Shu Chien, University of California at San Diego, La Jolla, CA, and approved September 15, 2006 (received for review May 19, 2006)

Mesenchymal stem cells (MSCs) are a potential source for the construction of tissue-engineered vascular grafts. However, how vascular mechanical forces regulate the genetic reprogramming in MSCs is not well understood. Mechanical strain in the vascular wall is anisotropic and mainly in the circumferential direction. We have shown that cyclic uniaxial strain on elastic substrates causes the cells to align perpendicularly to the strain axis, which is different from that in the vascular wall. To simulate the vascular cell alignment and investigate the anisotropic mechanical sensing by MSCs, we used soft lithography to create elastomeric membranes with parallel microgrooves. This topographic pattern kept MSCs aligned parallel to the strain axis, and the cells were subjected to 5% cyclic uniaxial strain (1 Hz) for 2–4 days. DNA microarray analysis revealed global gene expression changes, including an increase in the smooth muscle marker calponin 1, decreases in cartilage matrix markers, and alterations in cell signaling (e.g., down-regulation of the Jagged1 signaling pathway). In addition, uniaxial strain increased MSC proliferation. However, when micropatterning was used to align cells perpendicularly to the axis of mechanical strain, the changes of some genes were diminished, and MSC proliferation was not affected. This study suggests that mechanical strain plays an important role in MSC differentiation and proliferation, and that the effects of mechanotransduction depend on the orientation of cells with respect to the strain axis. The differential cellular responses to the anisotropic mechanical environment have important implications in cardiovascular development, tissue remodeling, and tissue engineering.

stem cell engineering | differentiation | genetic reprogramming | uniaxial mechanical strain | micropatterning

The availability of suitable and abundant cell sources is one of the limiting factors in vascular tissue engineering (1). Human mesenchymal stem cells (MSCs) represent a potential source for generating mesenchyme cells in the vascular wall, e.g., smooth muscle cells (SMCs), for the construction of vascular grafts. MSCs derived from bone marrow are nonhematopoietic and pluripotent, and they have the ability to differentiate into a variety of cell types, including SMCs (2–4). Additionally, studies have shown that MSCs have minimal immunogenic response *in vivo*, making them potentially suitable for allogeneic transplantation into human patients (5). Previous work has shown that when MSCs are transplanted into the heart, they can differentiate into SMCs and contribute to vascular remodeling (6, 7), suggesting that certain microenvironmental cues may be important in promoting differentiation to a SMC phenotype. However, the effects of vascular microenvironmental factors on MSCs are not yet well understood.

In particular, *in vivo* mechanical stimuli within blood vessel walls may play an important role in MSC differentiation into a vascular SMC phenotype. Previous work has shown that mechanical strain has an effect on proliferation and differentiation of vascular SMCs, including up-regulation of various SMC contractile markers (8–10), and the cells aligned perpendicularly to the axis of strain (11). Similarly, we have shown that when MSCs are subjected to conditions of cyclic uniaxial strain on silicone membranes, the cells show an initial up-regulation of SMC markers that eventually drops back to basal levels after the cells align perpendicularly to the axis of strain as a means of reducing the effective stress on their cytoskeleton (12). This cellular orientation differs from *in vivo* conditions where vascular SMCs align in the circumferential direction (13, 14) or, in some cases, in a helical pattern (15) in the arterial wall and SMCs are subject to circumferential cyclic strain because of the pulsatile nature of the blood pressure. To better mimic these *in vivo* conditions and compare the cellular responses to uniaxial strain in different directions, we used micropatterning techniques to keep the cells aligned in one direction and investigated the anisotropic mechanical sensing by MSCs.

Micropatterning techniques have been used as a powerful tool to control cell spreading, morphology, and functions (16–19). Our previous work with micropatterned poly(dimethyl siloxane) (PDMS) membranes with parallel microgrooves under static culture conditions has shown that cells will align with these grooves via contact guidance, similarly to how cells align along collagen fibers *in vivo* (20). However, it is unclear whether cells will retain this alignment during cyclic uniaxial strain (Fig. 6, which is published as supporting information on the PNAS web site). In the current study, we used soft lithography to create elastomeric PDMS membranes with parallel 10-μm microgrooves to control cell alignment.

DNA microarray offers a powerful tool to analyze global genetic reprogramming (21). We demonstrated that micropatterned guidance helped maintain MSC alignment with the axis of strain, and subsequent microarray analysis revealed global gene expression changes including an increase in the smooth muscle marker calponin 1, decreases in cartilage matrix markers, alterations in cell-signaling pathways, and changes in several genes involved in cell-cycle control. These changes were further verified with quantitative RT-PCR (qRT-PCR), Western blotting, and fluorescent-activated cell sorting (FACS) cell-cycle analysis. However, when the same micropatterned guidance was used to align MSCs perpendicularly to the axis of strain, some of the strain-induced effects were partially attenuated, including reduced changes in matrix remodeling and cell signaling, and no significant changes in cell proliferation were induced. Together,

Author contributions: K.K. and S.L. designed research; K.K. and J.C. performed research; K.K. and C.H. contributed new reagents/analytic tools; K.K. and J.C. analyzed data; and K.K. and S.L. wrote the paper.

The authors declare no conflict of interest.

This article is a PNAS direct submission.

Abbreviations: MSC, mesenchymal stem cell; SMC, smooth muscle cell; PDMS, poly(dimethyl siloxane); qRT-PCR, quantitative RT-PCR; ECM, extracellular matrix; LOX, lysyl oxidase; MMP1, matrix metalloproteinase 1; BGN, biglycan; COL10A1, collagen type X α1; COL11A1, collagen type XI α1; COMP, cartilage oligomeric matrix protein; GPCR5A, G protein-coupled receptor 5A; ARL7, ADP ribosylation factor-like protein 7; JAG1, jagged 1; HES1, hairy and enhancer of split 1; SDC1, syndecan 1; ANGPT1, angiopoietin 1; EGR2, early growth response 2; CDKN1C, cyclin-dependent kinase inhibitor 1C; PI, propidium iodide.

‡To whom correspondence should be addressed at: Department of Bioengineering, University of California, 471 Evans Hall, Berkeley, CA 94720-1762. E-mail: song_li@berkeley.edu.

© 2006 by The National Academy of Sciences of the USA

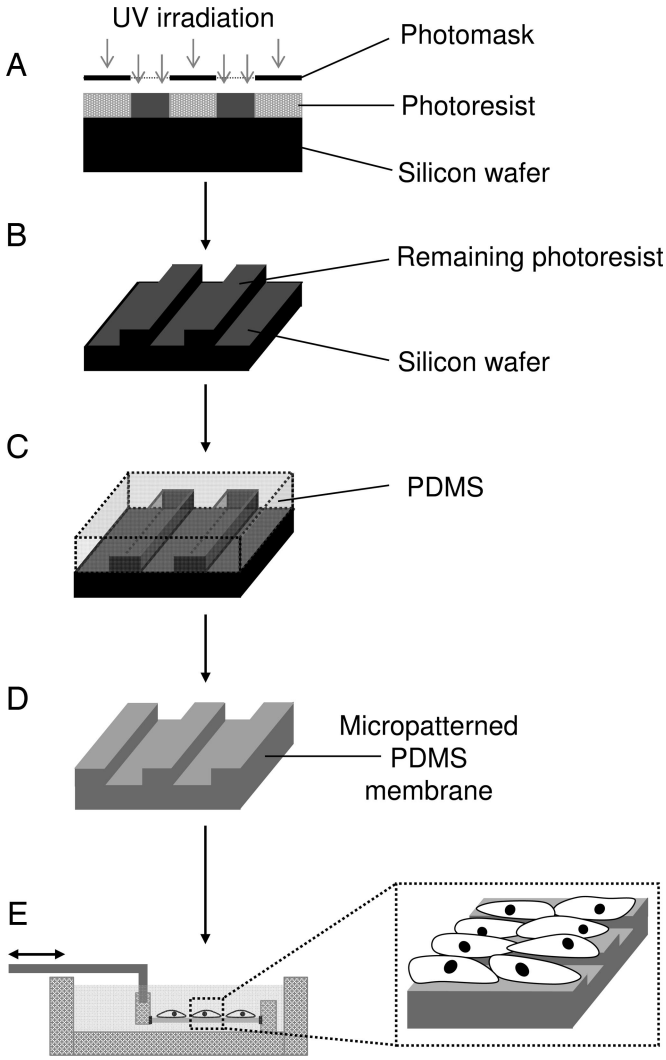

Fig. 1. Microfabrication of patterned membranes and the assembly into stretch chambers. (*A*) Negative photoresist was spin-coated onto a silicon wafer and exposed to UV irradiation through patterned photomask. (*B*) Unpolymerized photoresist was washed away. (*C*) PDMS (plus initiator) was poured on patterned silicon wafer and spun to desired thickness, degassed, cured at 70°C, and resulted in a micropatterned membrane. (*D*) PDMS membrane is removed from wafer. (*E*) Membrane is O_2 plasma-treated, coated with collagen I, and assembled into custom-built polysulfone stretch chambers. MSCs were seeded on a micropatterned surface and allowed to grow overnight. Stretch machine was started after 24 h to apply cyclic strain (5%, 1 Hz, 2–4 days).

these results suggest that mechanical stimulation with cyclic uniaxial strain may play a role in MSC differentiation and proliferation, and that the effects of mechanotransduction depend on the orientation of cells with respect to the strain axis.

Results

Parallel-Oriented Microgrooves Maintained Cell Alignment During Cyclic Uniaxial Strain. The elastic PDMS membranes with parallel microgrooves (10 μm in width, 3 μm in height) were fabricated and assembled into the mechanical stretch device as shown in Fig. 1 (see *Materials and Methods* for detail). To determine the effects of uniaxial mechanical strain on cell alignment on elastic substrates with and without microgrooves, MSCs were subjected to cyclic uniaxial strain within physiological range (5%, 1 Hz) for 2 days. Confocal microscopy of actin filaments showed that MSCs aligned perpendicular to the axis of mechanical strain on

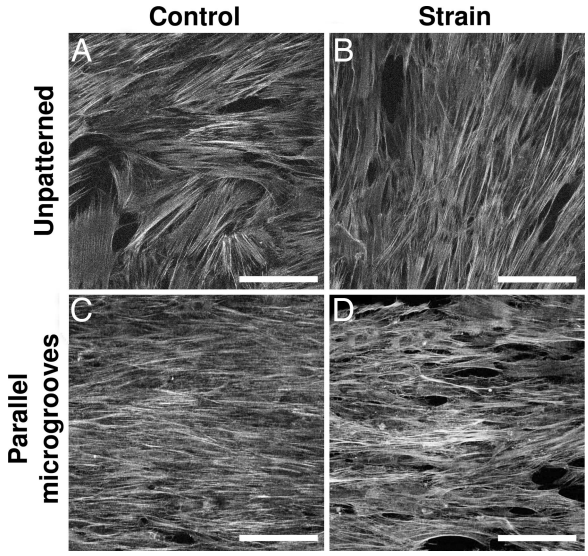

Fig. 2. F-actin filaments in MSCs after 2 days of cyclic uniaxial strain (5%, 1 Hz; strain was in left→right direction). The cells on unpatterned membranes had random fiber orientation (*A*), whereas strained cells on unpatterned membranes showed perpendicular alignment with strain (*B*). In *C* and *D*, micropatterned grooves were aligned parallel to the axis of strain. Note that strained cells on parallel-patterned membranes remained aligned with the axis of strain (*D*). (Scale bars, 100 μm.)

unpatterned elastic substrate (Fig. 2 *A* and *B*). On micropatterned PDMS membranes, MSCs covered the entire surface and aligned with the microgrooves (Fig. 2*C*), indicating that MSCs spread over the shallow microgrooves and follow the topographic guidance. Under uniaxial strain, MSCs on parallel microgrooves remained well aligned with the microgrooves and the axis of strain (Fig. 2*D*). Although cell alignment is maintained on micropatterned membranes, overall intensity and structure of F-actin did not show significant changes between control and strain conditions on both patterned and unpatterned membranes. Vinculin staining of focal adhesions demonstrated that focal adhesions aligned the same way as actin filaments in response to mechanical strain (Fig. 7, which is published as supporting information on the PNAS web site).

Cyclic Uniaxial Strain Caused Genetic Reprogramming in MSCs. To determine mechanical strain-induced genetic reprogramming in MSCs, we profiled the gene expression by using DNA microarrays. MSCs were seeded on micropatterned membranes with microgrooves parallel to the axis of strain and subjected to cyclic uniaxial strain (5%, 1 Hz) for 2 days. RNA samples were used for microarray analysis, and signal intensity was analyzed for statistical significance and sorted by fold change (ratio of "strain/control"). Log-scale scatter plots of signal intensity values from all 22,944 probe sets from each set of microarray hybridizations showed that most genes remain relatively unchanged by cyclic uniaxial strain (Fig. 8, which is published as supporting information on the PNAS web site). Using fold-change cutoff values of $\geq$1.50 or $\leq$0.67 and a P value cutoff of $<$0.05, we found that of 22,944 total probe sets, 254 met these criteria. Because some genes are repeated as multiple probe sets on a microarray chip, these probe sets corresponded to 197 unique genes (see Tables 1 and 2, which are published as supporting information on the PNAS web site). Of these 197 genes, 76 were up-regulated by cyclic uniaxial strain and 121 were down-regulated. For brevity, 50 of these genes are listed in Table 1, including those involved in smooth muscle contractility,

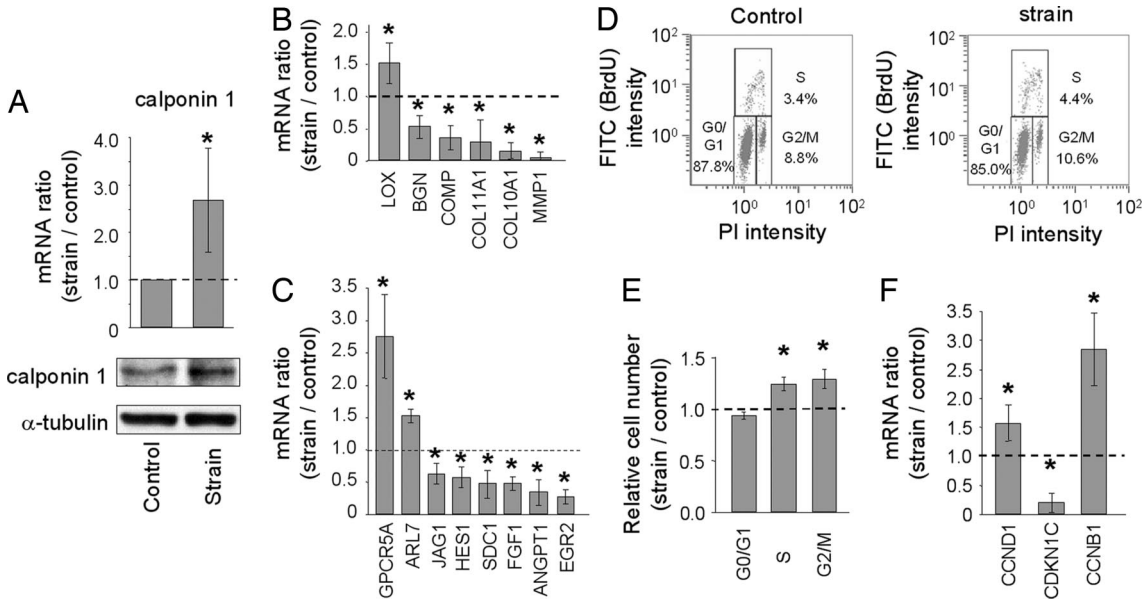

Fig. 3. Verification of changes from microarray analysis. Cyclic uniaxial strain (5%, 1 Hz, in parallel to microgrooves) was applied to MSCs for 2 days (for qRT-PCR and cell-cycle analysis) or 4 days (for protein expression analysis). (*A*) qRT-PCR and Western blot analyses showing increase in calponin 1 gene and protein expression after 2 and 4 days, respectively. α-tubulin is equal loading control. (*B*) qRT-PCR data showing relative expression changes of ECM-related genes after cyclic strain. (*C*) qRT-PCR data showing relative expression changes of cell-signaling molecules after cyclic strain. (*D*) FACS dot plots showing percentage of cells in each phase of cell cycle after 2 days of cyclic strain experiments. (*E*) Quantification of FACS cell cycle data. (*F*) qRT-PCR data showing relative changes in cell-cycle genes. *, $P < 0.05$ in comparison to respective control by using log-transformed one-sample *t* test, $n \geq 3$. CCND1, cyclin D1; CCNB1, cyclin B1.

proliferation, extracellular matrix (ECM) remodeling, and cell signaling.

Cyclic Uniaxial Strain with Parallel Cell Alignment Increased Contractile Marker Calponin 1 and Decreased Cartilage Matrix Proteins. We first verified the change of the SMC contractile marker calponin 1. According to microarray data, cyclic uniaxial strain with parallel-oriented microgrooves caused a 2.11-fold increase in calponin 1 gene expression (Table 1). Using qRT-PCR and Western blotting analyses, we found a 2.68-fold increase in calponin 1 gene expression after 2 days and a nearly 60% increase in protein expression after 4 days (Fig. 3*A*).

The microarray results suggested that uniaxial strain significantly affected ECM remodeling. The verification of selected genes with qRT-PCR confirmed the changes (Fig. 3*B*). Uniaxial strain increased lysyl oxidase (LOX) for cross-linking fibrous collagens and elastins and drastically decreased matrix metalloproteinase 1 (MMP1) by >90%, suggesting a coordinated enhancement of fibrous matrix assembly. In contrast, uniaxial strain caused decreases in several chondrogenic/osteogenic ECM genes such as biglycan (BGN), collagen type X α1 (COL10A1), collagen type XI α1 (COL11A1), and cartilage oligomeric matrix protein (COMP) (Fig. 3*B*), and an increase in aggrecanase ADAMTS5 (Table 1). These results strongly suggest that uniaxial strain promotes the phenotype of tension-bearing tissue but suppresses the phenotype of compression-bearing tissues.

Cyclic Uniaxial Strain with Parallel Cell Alignment Regulated the Expression of Signaling Molecules. The gene expression of several cell-signaling molecules was regulated by uniaxial strain. Uniaxial strain induced the expression of G protein-coupled receptor 5A (GPCR5A) and ADP ribosylation factor-like protein 7 (ARL7), while decreasing the gene expression of Notch ligand Jagged 1 (JAG1) and Notch pathway effector hairy and enhancer of split 1 (HES1) (Fig. 3*C*). We postulated that the decrease of JAG1 by uniaxial strain caused the decrease of HES1. Indeed, knocking down JAG1 (70–80% inhibition) with JAG1 siRNA (Dharmacon, Lafayette, CO) decreased HES1 gene expression by ≈50% (data not shown), suggesting that the decrease of JAG1 by uniaxial strain down-regulates Notch pathway signaling.

In addition, uniaxial strain decreased the expression of syndecan 1 (SDC1), fibroblast growth factor 1 (FGF1), angiopoietin 1 (ANGPT1), and early growth response 2 (EGR2) (Fig. 3*C*). Because SDC1 regulates FGF2 binding and activity (22), the decrease of SDC1 and FGF1 suggests that uniaxial strain down-regulates FGF1 and FGF2 signaling.

Cyclic Uniaxial Strain with Parallel Cell Alignment Increased MSC Proliferation. Data from the microarray showed that uniaxial strain caused 1.88- and 1.78-fold increases in cyclins B1 and B2, respectively (Table 1), suggesting an increase in MSC proliferation. Based on this data, we investigated changes in MSC cell cycle after stimulation with cyclic uniaxial strain on parallel-oriented microgrooves. FACS analysis revealed slight increases in the relative number of cells in the S phase and G_2/M phases after stimulation with cyclic uniaxial strain (Fig. 3 *D* and *E*). We also used qRT-PCR to verify increases in gene expression of cyclins B1 and B2 and found 2.84-fold (Fig. 3*F*) and 1.76-fold (data not shown) increases, respectively. The increase of cyclins B1 and B2 is correlated with G_2/M phase activity. To determine the expression of genes involved in S phase, we investigated gene expression of cyclin D1, which is required for the G_1/S transition, and cyclin-dependent kinase inhibitor 1C (CDKN1C), which acts as an inhibitor of G_1 cyclin/Cdk complexes. qRT-PCR revealed a statistically significant increase of cyclin D1 and decrease of CDKN1C (Fig. 3*F*), consistent with the increase of MSC proliferation by uniaxial strain.

Perpendicular-Oriented Microgrooves Altered Effects of Uniaxial Strain on MSCs. To investigate whether cellular orientation plays a role in MSC response to uniaxial strain, we used the same micropatterned membranes but with the microgrooves aligned perpendicularly to the axis of strain. As shown in Fig. 4*A*, MSCs

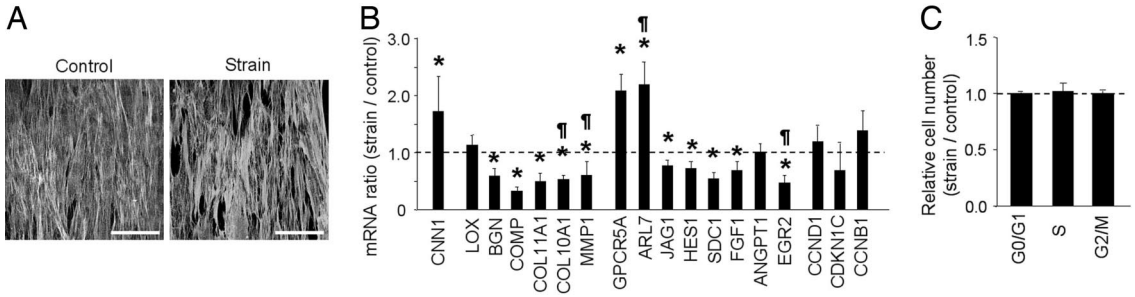

Fig. 4. Differential responses to cyclic uniaxial strain when microgrooves are oriented in perpendicular to uniaxial strain axis. Cyclic uniaxial strain (5%, 1 Hz) was applied to MSCs for 2 days. (*A*) F-actin filaments in MSCs on membranes with perpendicular-oriented microgrooves (5%, 1 Hz; uniaxial strain was left→right; microgrooves were up→down). (Scale bars, 100 μm.) (*B*) Comparison of gene expression in response to uniaxial strain in perpendicular to cell alignment axis. *, $P < 0.05$ in comparison to respective unstrained control by using a log-transformed one-sample *t* test, $n \geq 3$. ¶, $P < 0.05$ in comparison to respective control (unstrained) and to the ratio (strain/control) in response to uniaxial strain in parallel to cell alignment axis using a two-tailed *t* test, $n \geq 3$. (*C*) Relative changes of cell cycle in response to uniaxial strain perpendicular to cell alignment axis. CNN1, calponin 1; CCNB1, cyclin B1.

aligned with the microgrooves under control conditions and remained aligned under uniaxial strain in the perpendicular direction. Note that this alignment during uniaxial strain is similar to that on unpatterned membranes (Fig. 2*B*). Vinculin staining showed the alignment of focal adhesions on microgrooves with or without uniaxial strain (Fig. 9, which is published as supporting information on the PNAS web site).

When MSCs were oriented perpendicular to the axis of uniaxial strain, calponin 1 gene expression still was increased significantly by uniaxial strain, although to a lesser extent (≈1.7-fold) (Fig. 4*B*). LOX expression had no induction, and MMP1 was suppressed to a lesser extent. Perpendicular uniaxial strain significantly decreased cartilage matrix markers BGN, COMP, COL11A1, and COL10A1, except that the decrease of COL10A1 was significantly less in comparison to that under uniaxial strain with parallel cell alignment. These results suggest that the collagen assembly may be sensitive to the direction of uniaxial strain and that the expression of tension- and compression-bearing tissue markers is affected only partially by strain direction.

The expression of most signaling molecules, except ANGPT1, was regulated the same way regardless of the strain direction (Fig. 4*B*). The decrease of EGR2 was less dramatic under perpendicular uniaxial strain than that under parallel uniaxial strain. Interestingly, one gene (ARL7) increased more with perpendicular uniaxial strain.

In contrast, cell cycle-related genes (cyclin D1, cyclin B1, and CDKN1C) were not regulated by uniaxial strain in the perpendicular direction (Fig. 4*B*). Consistently, FACS analysis revealed that cyclic uniaxial strain in the perpendicular direction did not affect MSC proliferation (Fig. 4*C*), which is in contrast to the increase in proliferation under cyclic uniaxial strain with parallel cell alignment (Fig. 3*E*).

Discussion

The majority of investigations involving vascular SMC differentiation with mechanical stimulation in two-dimensional culture have examined the effects of cyclic equiaxial strain, in which cells are strained uniformly in all directions (23). Several studies have shown that SMC response to this stimulus involves up-regulation of smooth muscle markers such as h-caldesmon (8), SM-1/2 (24), and SM α-actin (9). However, our previous study revealed a decrease in the smooth muscle markers SM α-actin and SM22 when MSCs were stimulated with cyclic equiaxial strain (12).

In contrast to equiaxial strain, uniaxial or anisotropic strain provides a mechanical stimulus more similar to *in vivo* conditions of circumferential strain within a blood vessel wall. However, when MSCs are stimulated with cyclic uniaxial strain on unpatterned silicone membranes, the cells aligned in the perpendicular direction, which affected the stress applied to the cells and thus the cell responses (12, 23). In this study, we have shown that micropatterning techniques can be used to keep MSCs aligned with the axis of strain and simulate the guidance of cells by matrix fibrils. This alignment is well maintained after 2 days of cyclic strain (Fig. 2) and remains stable after 4 days of strain (data not shown). Thus, these micropatterned membranes help to better mimic *in vivo* microenvironmental conditions of circumferential or helical SMC alignment within a blood vessel wall, and provide an additional control compared with current methods of mechanical stimulation. This will be a valuable system to investigate anisotropic mechanosensing by vascular cells and stem cells.

A major finding using the genetic profiling approach is the differential effects of uniaxial strain on the phenotype markers of SMCs and cartilage (Fig. 5). Uniaxial strain increased the contractile marker calponin but not SMC mature marker myosin heavy chain, suggesting that additional factors (e.g., soluble factors) may be required to drive the terminal differentiation of MSCs. The increase of LOX and decrease of MMP1 suggest that uniaxial strain promotes the assembly of matrix fibrils, which depends on the direction of uniaxial strain. In contrast, the cartilage matrix proteins were decreased significantly by uniaxial strain, suggesting that tensile stress suppresses the phenotype of

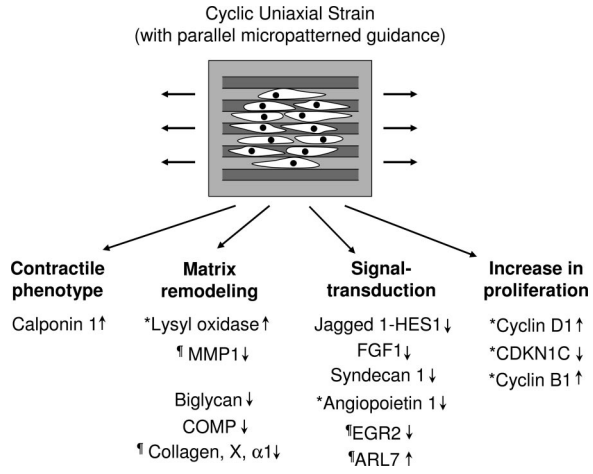

Fig. 5. Overview of changes induced in MSCs by cyclic uniaxial strain with parallel orientation. The genes that were not affected by uniaxial strain in perpendicular to cell alignment axis are marked with an asterisk. The genes that were regulated the same way regardless of strain direction but the magnitudes of changes were dependent on strain direction are marked with ¶.

compression-bearing tissue. Our study provides an explanation at the molecular level that different kinds of mechanical forces may have differential effects on tissue phenotype.

Another major finding is the heterogeneous responses of different genes to the direction of uniaxial strain. Although many genes responded the same way regardless of the axis of uniaxial strain, some of the genes (e.g., LOX, MMP1, COL10A1, ARL7, ANGPT1, EGR2, and cell cycle-related genes) did respond differently. In general, these genes either did not change (e.g., LOX, ANGPT1, and cell cycle-related genes) or had less change (MMP1, COL10A1, and EGR2) in response to uniaxial strain in perpendicular to cell alignment axis. Interestingly, one gene (ARL7) had a greater change when MSCs were oriented perpendicular to the strain. These results suggest three possibilities: (*i*) gene expression is not sensitive to the direction of uniaxial strain, (*ii*) gene expression is more sensitive to the uniaxial strain in parallel to cell alignment axis, and (*iii*) gene expression is more sensitive to the uniaxial strain perpendicular to cell alignment axis. This anisotropic mechanosensing may be related to specific genes and upstream signaling, and may be cell-type dependent. For example, there was more increase of α-actin expression in tendon fibroblasts in response to uniaxial strain in the direction of cell alignment (25), whereas there was more actin assembly and higher expression of atrial natriuretic factor, connexin-43, and *N*-cadherin in cardiac myocytes in response to greater principal strain in perpendicular to cell alignment axis (26).

One explanation of heterogeneous responses of genes to anisotropic mechanical strain is that the upstream signaling cascades leading to the expression of different genes involve different mechanosensing mechanisms. For example, if a signaling pathway is regulated by the changes of cell membrane deformation, cell spreading area, and/or cell volume, it may be less sensitive to the direction of uniaxial strain. On the other hand, if a signaling pathway is regulated by the force transduction through cytoskeleton and focal adhesions, it may be more sensitive to the direction of uniaxial strain. This hypothesis warrants further investigations in the future.

Overall, this study has shown that micropatterning techniques can be used to better mimic *in vivo* conditions within *in vitro* cell culture systems and to investigate anisotropic mechanosensing in stem cells and other cell types. This work has far-reaching implications in terms of MSC differentiation under mechanical stimuli in bioreactors or upon implantation within vascular grafts, and it provides a basis for creating new *in vitro* cell culture systems for stem cell and tissue engineering. Furthermore, some results could be extrapolated for vascular biology. For example, the alignment of the cells mimics the organization of SMCs *in vivo* (aligned in the circumferential direction or in the helical pattern). Uniaxial strain or anisotropic strain can be applied to cells in any direction to simulate the mechanical strain in *in vivo*. The increase of contractile markers and the decrease of cartilage markers by uniaxial strain suggest that the tension-bearing tissue phenotype is promoted, which is consistent with previous findings in SMCs. The anisotropic mechanosensing by cells suggest that how mechanical strain is applied to the cells does affect cell response. This finding remains to be verified in SMCs. Elucidating the anisotropic mechanosensing of cells will help us to understand the roles of mechanical strain in different directions in vascular remodeling and to design better bioreactors for vascular tissue engineering.

Materials and Methods

Microfabrication and Soft Lithography. To create patterned membranes with parallel microgrooves (10 μm wide, 3 μm deep, 10 μm distance between each groove), we used microfabrication techniques outlined in Fig. 1. Photoresist (OIR 897-10I; Arch Chemicals, Norwalk, CT) was spin-coated onto a silicon wafer, and a patterned photomask was used to expose the photoresist to UV light. After washing away the unpolymerized photoresist, PDMS was prepared according to the manufacturer's protocol (Sylgard 184; Dow Corning, Midland, MI), spin-coated onto the patterned silicon wafers to desired thickness ($\approx$250 μm), degassed under vacuum, and cured at 70°C for 1 h. The resulting micropatterned membranes were removed from the template, cut to appropriate dimensions (for assembly into custom-built stretch chambers), and thoroughly washed and sonicated before use. The surface topography of micropatterned PDMS membranes was examined by scanning electron microscopy (27). Mechanical testing showed that PDMS membranes were elastic under cyclic uniaxial strain (<30% strain, 1 Hz).

Cell Culture and Cyclic Uniaxial Strain. Human MSCs were acquired from Cambrex (East Rutherford, NJ) and cultured in MSC growth medium (Cambrex) for expansion without differentiation. After cell expansion, MSCs were subjected to flow cytometry analysis of surface marker expression (positive for CD105, CD166, CD29, and CD44 and negative for CD34, CD14, and CD45) to confirm the undifferentiated state of MSCs (28). Cells were kept in a humidified incubator at 37°C and supplemented with 5% CO_2. For strain experiments, micropatterned membranes were O_2 plasma-treated with a Plasma-Prep II plasma etcher (Structure Probe, West Chester, PA) for 1 min and coated with a collagen I, rat tail (BD Biosciences, Bedford, MA) solution (0.8 mg/ml in 0.1% acetic acid). Membranes were assembled into custom-built uniaxial stretch chambers (Fig. 2) with microgrooves oriented either parallel or perpendicular to the axis of strain as stated for each experiment. MSCs were seeded at confluency on the patterned surfaces and supplemented with DMEM (10% FBS/1% penicillin-streptomycin/1% fungizone) and 10% CO_2 in a humidified incubator. For samples subjected to uniaxial strain, the polysulfone bar at one end of the chamber was attached to a motorized cam/rotor system, while the other end of the frame remained stationary, thereby stretching the membrane (Fig. 1). For controls, the polysulfone bar still moved back and forth, but the other end of the frame was not held stationary so that the entire membrane moved without being strained. This effect accounted for possible fluid disturbance in the stretch chamber. MSCs were subjected to conditions of 5% cyclic uniaxial strain at a frequency of 1 Hz for 2 days (unless otherwise noted).

Immunofluorescent Staining and Confocal Microscopy. Immunostaining and confocal microscopy were used to visualize the structure of cytoskeleton and focal adhesions in MSCs. MSCs were fixed with 4% paraformaldehyde, permeabilized with 0.5% Triton X-100, and blocked with 1% BSA. For cytoskeletal staining, samples were incubated in rhodamine-conjugated phalloidin (Molecular Probes, Eugene, OR) for 30 min to stain all filamentous actin (F-actin). For staining of focal adhesions, samples were incubated in anti-vinculin primary antibody (Sigma, St. Louis, MO) for 1 h, followed by incubation with FITC-conjugated anti-mouse IgG secondary antibody (Jackson ImmunoResearch, West Grove, PA) for 1 h.

We used a Leica (Wetzlar, Germany) True Confocal Scanner SL confocal microscopy system, including He/Ne laser sources and a Leica DM IRB microscope, to capture multiple *Z*-section images ($\approx$0.3- to 0.5-μm-thick sections over a range of $\approx$6 μm) for a given specimen. These sections subsequently were projected to a single plane to create an overall image of the specimen. All images in a given group were collected with the same hardware and software settings.

RNA Isolation, Oligonucleotide Microarray, and qRT-PCR. Cells were lysed with 1.0 ml of RNA STAT-60 reagent (Tel-Test, Friendswood, TX) per membrane. RNA was extracted by using chloroform and phenol extractions and precipitated by using isopropanol, and the resulting RNA pellet was washed with 75% ethanol. For microarray analysis, the RNA pellet was resuspended in 12 μl of nuclease-free H_2O and analyzed with a UV spectrophotometer to confirm purity

of $A_{260}/A_{280} \geq 1.80$. RNA concentration was determined by using the RiboGreen quantification assay (Molecular Probes, Carlsbad, CA), and samples subsequently were diluted to a concentration of 0.50 mg/ml. Then, 10 μl of each sample was submitted to a core facility for analysis with an Affymetrix (Santa Clara, CA) oligonucleotide microarray U133AAofAv2 chip containing 22,944 probe sets per chip. Samples were labeled and hybridized according to Affymetrix protocols. Signal intensities were obtained for all probe sets and were organized by using GeneTraffic version 3.2 microarray analysis software (Iobion, La Jolla, CA).

For qRT-PCR, RNA pellets were resuspended in 20 μl of diethyl pyrocarbonate (DEPC)-treated H_2O and were quantified as described above. cDNA was synthesized by using two-step reverse transcription with the ThermoScript RT-PCR system (Invitrogen, Carlsbad, CA), followed by qRT-PCR with SYBR green reagent and the ABI Prism 7000 Sequence Detection System (Applied Biosystems, Foster City, CA). Primers for the genes of interest were all designed by using the ABI Prism Primer Express software version 2.0 (Applied Biosystems). Refer to Table 3, which is published as supporting information on the PNAS web site, for a full list of primer sequences. RNA from human SMCs, human MSCs, or human osteosarcoma cells was used to create standard curves for each gene, and gene levels from each sample were normalized to 18S levels from the same sample. Data were analyzed by using ABI Prism 7000 SDS software (Applied Biosystems).

Protein Isolation and Immunoblotting. Cells were lysed with 100 μl of lysis buffer [containing 25 mM Tris (pH 7.4), 0.5 M NaCl, 1% Triton X-100, 0.1% SDS, 1 mM PMSF, 10 μg/ml leupeptin, and 1 mM Na_3VO_4] per membrane. Protein lysates were centrifuged to pellet cellular debris, and the supernatant was removed and quantified by using the DC Protein Assay (Bio-Rad, Foster City, CA). Protein samples were run in SDS/PAGE and transferred to nitrocellulose membranes. Membranes were blocked with 3% nonfat milk and incubated with the primary antibody diluted in TBS-T buffer containing 25 mM Tris·HCl (pH 7.4), 60 mM NaCl, and 0.05% Tween 20. This was followed by incubation with either HRP-conjugated anti-mouse or anti-rabbit IgG secondary antibody (Santa Cruz Biotechnology, Santa Cruz, CA) as appropriate. To verify equal loading in all lanes, membranes subsequently were reprobed with one of the following antibodies diluted in TBS-T and followed again by incubation with antibody against α-tubulin (Santa Cruz Biotechnologies). Protein bands were visualized by using the ECL detection system (Amersham Biosciences, Piscataway, NJ), and signal intensity was analyzed by using Scion Image (Scion, Frederick, MD). The antibody against calponin 1 was from Sigma.

Analysis of Cell Proliferation. After 2 days of cyclic strain, MSCs were pulsed with 10 μM BrdU (Amersham Biosciences) for 1 h, released from the membranes by using 0.5% trypsin, and then fixed in 70% ethanol overnight at 4°C. MSCs then were incubated in 4 M HCl followed by permeabilization with 0.25% Triton X-100. MSCs then were incubated in anti-BrdU primary antibody (BD Biosciences) followed by incubation with FITC-conjugated anti-mouse IgG secondary antibody (Jackson ImmunoResearch). Lastly, the MSCs were stained with propidium iodide (PI; 10 μg/ml). Staining intensity was analyzed by using an Epics XL flow cytometer with EXPO32 ADC software (Beckman Coulter, Fullerton, CA). Individual cells were analyzed for side scatter, forward scatter, PI intensity, and FITC-BrdU intensity. Ten thousand single cells (cell clusters were excluded from analysis) were analyzed from each sample, and each cell was categorized into a phase of the cell cycle (G_1/G_0, S, or G_2/M) based on staining intensities. PI intensity determines DNA quantity in a given cell, whereas BrdU intensity gives a measure of DNA replication for that cell. To correct for baseline staining intensities and to avoid false-positive results, four staining controls were used: (*i*) MSCs with BrdU pulse and PI stain, (*ii*) MSCs with BrdU pulse but no PI, (*iii*) MSCs without BrdU pulse but with PI, and (*iv*) MSCs with neither BrdU pulse nor PI stain. All of these control groups were stained with the primary (anti-BrdU) and secondary (anti-mouse IgG) antibodies as described above.

Statistical Analysis. To account for baseline variations between experiments, values from an individual experimental sample were normalized to values from the corresponding control sample. After normalization, ratio values (strain/control) were pooled from all experiments and analyzed for statistical significance by using a log-transformed one-sample *t* test ($P < 0.05$, $n = 4$ for microarray, $n \geq 3$ for PCR, $n = 3$ for FACS). To determine statistical significance between parallel-oriented and perpendicular-oriented microgrooves under conditions of cyclic strain, ratio values from the two groups were compared by using a two-tailed *t* test ($P < 0.05$, $n \geq 3$ for PCR, $n = 3$ for FACS). Data were presented as mean ± SD.

We acknowledge Rahul Thakar, Mansoor Nasir, and Dorian Liepmann for help with the fabrication of the micropatterned wafers; Fanqing Chen and Heidi Feiler for help with microarray experiments; and Joanna So for general technical assistance. This work was supported by National Institutes of Health Grant HL078534.

1. Nerem RM, Seliktar D (2001) *Annu Rev Biomed Eng* 3:225–243.
2. Pittenger MF, Mackay AM, Beck SC, Jaiswal RK, Douglas R, Mosca JD, Moorman MA, Simonetti DW, Craig S, Marshak DR (1999) *Science* 284: 143–147.
3. Jiang Y, Jahagirdar BN, Reinhardt RL, Schwartz RE, Keene CD, Ortiz-Gonzalez XR, Reyes M, Lenvik T, Lund T, Blackstad M, *et al*. (2002) *Nature* 418:41–49.
4. Caplan AI, Bruder SP (2001) *Trends Mol Med* 7:259–264.
5. Koc ON, Lazarus HM (2001) *Bone Marrow Transplant* 27:235–239.
6. Mangi AA, Noiseux N, Kong D, He H, Rezvani M, Ingwall JS, Dzau VJ (2003) *Nat Med* 9:1195–1201.
7. Gojo S, Gojo N, Takeda Y, Mori T, Abe H, Kyo S, Hata J, Umezawa A (2003) *Exp Cell Res* 288:51–59.
8. Birukov KG, Shirinsky VP, Stepanova OV, Tkachuk VA, Hahn AW, Resink TJ, Smirnov VN (1995) *Mol Cell Biochem* 144:131–139.
9. Tock J, Van Putten V, Stenmark KR, Nemenoff RA (2003) *Biochem Biophys Res Commun* 301:1116–1121.
10. Li C, Xu Q (2000) *Cell Signal* 12:435–445.
11. Kaunas R, Nguyen P, Usami S, Chien S (2005) *Proc Natl Acad Sci USA* 102:15895–15900.
12. Park JS, Chu JS, Cheng C, Chen F, Chen D, Li S (2004) *Biotechnol Bioeng* 88:359–368.
13. Canham PB, Mullin K (1978) *J Microsc (Oxford)* 114:307–318.
14. Walmsley JG, Campling MR, Chertkow HM (1983) *Stroke* 14:781–790.
15. Rhodin J (1980) in *Handbook of Physiology*, ed Berne RM (Waverly, Baltimore), pp 1–31.
16. Whitesides GM, Ostuni E, Takayama S, Jiang X, Ingber DE (2001) *Annu Rev Biomed Eng* 3:335–373.
17. Folch A, Toner M (2000) *Annu Rev Biomed Eng* 2:227–256.
18. Chen CS, Tan J, Tien J (2004) *Annu Rev Biomed Eng* 6:275–302.
19. Tsang VL, Bhatia SN (2004) *Adv Drug Deliv Rev* 56:1635–1647.
20. Thakar RG, Ho F, Huang NF, Liepmann D, Li S (2003) *Biochem Biophys Res Commun* 307:883–890.
21. Brown PO, Botstein D (1999) *Nat Genet* 21:33–37.
22. Zhou FY, Owens RT, Hermonen J, Jalkanen M, Hook M (1997) *Eur J Cell Biol* 73:166–174.
23. Kurpinski K, Park J, Thakar RG, Li S (2006) *Mol Cell Biomech* 3:21–34.
24. Reusch P, Wagdy H, Reusch R, Wilson E, Ives HE (1996) *Circ Res* 79:1046–1053.
25. Wang JH, Yang G, Li Z (2005) *Ann Biomed Eng* 33:337–342.
26. Gopalan SM, Flaim C, Bhatia SN, Hoshijima M, Knoell R, Chien KR, Omens JH, McCulloch AD (2003) *Biotechnol Bioeng* 81:578–587.
27. Huang NF, Patel S, Thakar RG, Wu J, Hsiao BS, Chu B, Lee RJ, Li S (2006) *Nano Lett* 6:537–542.
28. Wang D, Park JS, Chu JS, Krakowski A, Luo K, Chen DJ, Li S (2004) *J Biol Chem* 279:43725–43734.